Why Ice Is So Slippery

Sigbjørn Løland Bore,[1,*] B. N. J. Persson,[2,3,4,†] and Henrik Andersen Sveinsson[5,‡]
[1]Hylleraas Centre for Quantum Molecular Sciences, Department of Chemistry, University of Oslo, PO Box 1033 Blindern, 0315 Oslo, Norway
[2]State Key Laboratory of Solid Lubrication, Lanzhou Institute of Chemical Physics, Chinese Academy of Sciences, 730000 Lanzhou, China
[3]Peter Grünberg Institute (PGI-1), Forschungszentrum Jülich, 52425, Jülich, Germany
[4]Multiscale Consulting, Wolfshovener Straße 2, 52428 Jülich, Germany
[5]The Njord Centre, Department of Physics, University of Oslo, PO Box 1048 Blindern, 0316 Oslo, Norway

(Received 15 January 2026; revised 30 May 2026; accepted 5 October 2026; published 18 November 2026)

We simulate nanoscale ice-glass friction from first principles and upscale it by modeling frictional heating. Nanoscale simulations alone overestimate friction and miss its velocity dependence. Frictional heating warms the contact toward the melting point, thickening the premelting film tenfold and cutting its viscosity a hundredfold; friction drops with velocity, matching experiment. Premelting forms the film without sliding or heating, but its slipperiness hinges on frictional heating, as Bowden and Hughes proposed in 1939, without melting. Snow, other materials, and coatings remain open.

DOI: 10.1103/9wv5-ypdm

The interest in ice friction has ancient roots, with early human activity involving sliding on ice from around 10 000 B.C. using sleds [1]. On this historical timescale, it was only very recently that the first scientific explanation for ice slipperiness was put forward in the 1800s by Michael Faraday's observations of premelting [2,3]: a liquid premelting film spontaneously forms on ice and provides lubrication. This explanation was followed by John Joly's pressure-melting theory [4]: pressure causes a melting point depression, creating a lubricating premelting film. Subsequently, Bowden and Hughes proposed that the low friction of ice results from frictional heating [5]: friction between a moving object on ice, such as a skate blade, generates heat, creating a thin film of liquidlike water on the ice surface. This water film acts as a lubricant, significantly reducing friction and enabling the smooth gliding motion characteristic of ice skating.

Modern science continues to debate the origin of ice friction. On the experimental side, Canale *et al.* emphasized the nanorheology of ice friction, measuring a viscoelastic interfacial film with a viscosity up to two orders of magnitude larger than that of bulk water and a rheology characteristic of a dense suspension [6]. Weber *et al.* combined friction experiments with molecular dynamics (MD) simulations, attributing ice slipperiness to highly mobile water molecules at the ice surface [7]. Liefferink *et al.* followed up, investigating the roles of temperature, pressure, and velocity, proposing a ploughing mechanism [8]. They concluded that the friction coefficient is not very sensitive to frictional heating. On the theoretical side, advances in computational efficiency have enabled MD studies of nanoscale ice friction. Using force-field MD simulations, Baran *et al.* found the premelting film to be a robust phenomenon, reporting shear thinning and large slip lengths at hydrophobic interfaces as crucial for low ice friction, arguing for a minor role of frictional heating due to low film viscosity [9,10]. More recently, Atila *et al.* performed ice sliding on ice MD simulations, proposing a mechanism for displacement-driven amorphization at low temperatures [11]. Their MD shows that a relatively thick (10 nm) liquidlike film can form at ice interfaces during slip with negligible temperature rise, through a competition between shear-induced amorphization and recrystallization. When sliding stops, the film recrystallizes, leaving only a few interfacial monolayers in nonice configurations set by the countersurface. Ice premelting at the ice-vapor interface has been observed in many experiments, but whether it also occurs at interfaces between ice and solids, in particular hydrophilic ones, is less well established. From these conflicting views, it can be concluded that no consensus has been reached on *why ice is so slippery.*

In this Letter, we present evidence that, at rocklike counterfaces, a premelting film forms without sliding or heating, and frictional heating is the primary cause of ice slipperiness. Applying machine-learning interatomic

*Contact author: s.l.bore@kjemi.uio.no
†Contact author: b.persson@fz-juelich.de
‡Contact author: h.a.sveinsson@fys.uio.no

Published by the American Physical Society under the terms of the Creative Commons Attribution 4.0 International license. Further distribution of this work must maintain attribution to the author(s) and the published article's title, journal citation, and DOI.

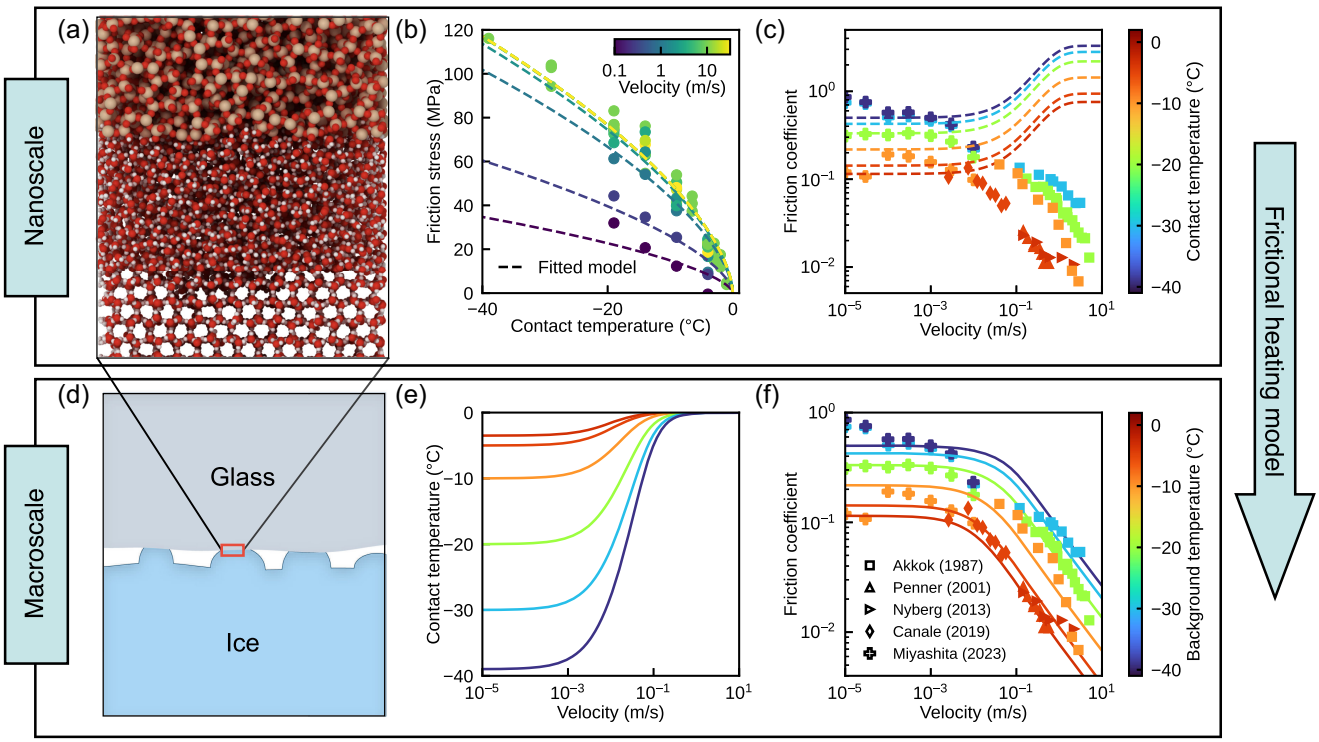


FIG. 1. Nanoscale vs macroscale ice friction. (a) Setup for nanoscale MD simulations of amorphous silica sliding on ice. (b) Friction stress as a function of contact temperature for different sliding velocities from nanoscale MD simulations, with fitted Eq. (1) (dashed lines). (c) Ice friction coefficient as a function of velocity for different temperatures with Eq. (1) directly, without frictional heating, comparing with experiments. (d) Illustration of macroscale friction, where nanoscale represents one asperity contact. (e) Contact temperature as a function of velocity for different background temperatures using the frictional heating model [Eq. (4)]. (f) Macroscale ice friction coefficient using the frictional heating model, comparing with experiments ($R^2_{\log} = 0.94$ on the full pool, $n = 88$; $R^2_{\log} = 0.88$ on the held-out validation subset at $v \geq 5 \times 10^{-3}$ m s^{-1}, $n = 55$, four sources—see End Matter). Contact temperatures for nanoscale MD simulations are reported in °C relative to the melting point of the model concerned: 289 K for DC-r^{2}SCAN and 270 K for TIP4P/Ice + ClayFF. Experimental friction coefficient data are from ice-glass friction experiments [6,42,43] and curling stone experiments [44,45], whose stones are composed of granite with a silica content of ~70%.

potentials (MLIPs) based MD, we simulate nanoscale ice friction against a realistic ice-glass (amorphous silica) interface—a model system for ice-rock contacts in nature—from first principles [see Fig. 1(a) and Supplemental Material [12] for details]. By integrating our nanoscale MD findings into the frictional heating model developed by Persson [41], we predict the macroscopic ice friction behavior. Comparing our macroscale predictions with experimental ice-glass friction data, we find excellent agreement, supporting the frictional heating theory of Bowden and Hughes.

The key control parameters in ice friction experiments are the background temperature T_0 of the ice and the velocity v of the sliding body. Direct prediction of experimental ice friction conditions using MD is impossible due to the large length and time scales involved. However, from nanoscale MD simulations, we can obtain the frictional shear stress $\sigma_f(v, T)$ acting in the asperity contact regions for given sliding velocity v and contact temperature T (see Supplemental Material [12]). We perform such simulations of the ice-glass contact [Fig. 1(a)], for $v \gtrsim 0.1$ m s^{-1}, with the friction stress shown in Fig. 1(b). The friction stress from nanoscale MD is well modeled by the following expression:

$$\sigma_f(v, T) = \sigma_k \left(1 - \frac{T}{T_m}\right)^{\beta} \left[1 - \left(1 - \frac{\sigma_c}{\sigma_k}\right) e^{-\frac{v}{v_k}}\right], \quad (1)$$

Equation (1) can be rationalized as a sigmoid between two limiting behaviors:

$$\sigma_f(v, T) = \sigma_c \left(1 - \frac{T}{T_m}\right)^{\beta}, \qquad v \ll v_k, \quad (2)$$

$$\sigma_f(v, T) = \sigma_k \left(1 - \frac{T}{T_m}\right)^{\beta}, \qquad v \gg v_k, \quad (3)$$

representing lower and upper velocity limits, respectively. Here, $\sigma_k = 391$ MPa, $v_k = 0.53$ m s^{-1}, and $\beta = 0.61$ are fit to our nanoscale MD friction-stress data for 0.1 m s^{-1} to 31.6 m s^{-1}, and $\sigma_c = 59$ MPa is anchored to the low-velocity ice-glass friction-coefficient data of Miyashita

et al. [42] at $v < 5 \times 10^{-3}$ m s^{-1}, where Eq. (1) reduces to Eq. (2) within ~5%. The four parameters are determined by an iterative cofit (End Matter). Equation (2) has previously been proposed by Persson for ice-ice friction experiments for low velocities [41], albeit with $\beta = 0.15$.

To incorporate heat transport effects, we use a frictional heating model. By assuming that ice and glass make contact at asperities, making up only a small fraction of the apparent contact area [Fig. 1(d)], the contact temperature can be expressed as [41,46] (see End Matter for additional details)

$$T = T_0 + \sigma_f(v,T)\frac{s(v)vR_p}{\kappa}\left(1+\frac{\pi}{8}\frac{R_p v}{D}\right)^{-\frac{1}{2}}. \quad (4)$$

Here, R_p is the asperity contact radius, D is the thermal diffusivity, and κ is the thermal conductivity, all of which are available from literature data (see Table I). $s(v)$ is the proportion of heat that is absorbed by the slider, and it can be explicitly expressed as a function of the sliding velocity (see End Matter), typically in the range from 0.6 to 1 with increasing sliding velocity. By inserting Eq. (1) into Eq. (4), we obtain an implicit equation for the contact temperature at a given background temperature and sliding velocity, which we solve iteratively to obtain T and σ_f. Of the four parameters in Eq. (1), only σ_c is anchored to experiment—specifically, Miyashita *et al.* [42] at $v < 5 \times 10^{-3}$ m s^{-1}; σ_k, v_k, and β are fit to our nanoscale MD simulations (see End Matter). The friction coefficient can then be estimated from friction stress as $\mu = \sigma_f/\sigma_P$ by assuming that contact pressure equals ice penetration hardness, with $\sigma_P \simeq 35$ MPa (see End Matter).

Figure 1(c) reports the nanoscale ice friction coefficient as a function of sliding velocity for different temperatures, using the nanoscale MD results directly. When compared with experimental ice friction data, the coefficient of friction not only is grossly overestimated in magnitude but also shows the wrong trend: friction increasing with sliding velocity, in opposition to experiments. Using the frictional heating model described by Eq. (4), we can upscale nanoscale MD results to the macroscale. The resulting contact temperature is reported in Fig. 1(e). At low velocities, frictional heating is negligible, with the contact temperature close to the background temperature. At higher velocities, frictional heating increases the contact temperature, which approaches the melting point for a sliding velocity of around 0.1 m s^{-1}. This change in contact temperature dramatically changes the ice friction coefficient behavior from the nanoscale ice friction coefficients in Fig. 1(c) to the macroscale ice friction coefficients in Fig. 1(f), which shows excellent agreement with experimental data [6,42–45], having an R^2_{log} coefficient of determination of 0.94 over the full experimental pool ($n = 88$) and 0.88 on a held-out validation subset of $n = 55$ points from four sources (Akkok, Penner, Nyberg, Canale) at $v \geq 5 \times 10^{-3}$ m s^{-1}, where the macroscale prediction is independent of the σ_c anchor (see End Matter).

From the nanoscale MD simulations, we can extract properties of the premelting film, which we can also upscale to the macroscale using the frictional heating model. In Fig. 2(a), we report the premelting film thickness as a function of sliding velocity. The premelting film thickness increases with sliding velocity at the nanoscale, but the effect is significantly amplified at the macroscale, rising by about an order of magnitude. At fixed contact temperature the film thickens by only a factor of 2.4 to 3.8 across the simulated velocity range, 0.1 to 31.6 m s^{-1}: shear-induced disordering advances with sliding distance [11,49,50], whereas recrystallization proceeds thermally, at a rate set by temperature rather than by the sliding, so faster sliding disorders the interface faster, the recovery rate is unchanged, and the steady-state thickness grows with velocity. The much larger macroscale amplification is thermal: frictional heating drives the contact toward T_m, where recrystallization slows steeply, and at 10 m s^{-1}, when the contact temperature goes from −19 °C to −1 °C, the film thickens by a further factor of ~3. This amplification is also evident when considering viscosity, which drops by about two orders of magnitude. It is these two effects combined that cause the strong drop in ice friction with increasing sliding velocity at the macroscale.

The validity of our findings rests on several factors, whose robustness we quantify in Fig. 3. First,

TABLE I. Material properties used in the frictional heating model. Granite properties were obtained from Ref. [47], and ice properties were from Ref. [48].

Property	Unit	Ice	Granite
Thermal conductivity κ	(W m^{-1} K^{-1})	2.2	3.2
Density ρ	(g cm^{-3})	0.917	2.7
Specific heat C_P	(J kg^{-1} K^{-1})	2100	800

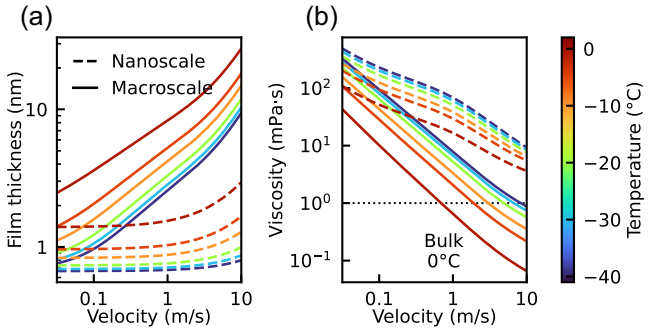


FIG. 2. Nanoscale vs macroscale premelting film properties. (a) Premelting film thickness and (b) viscosity estimated directly from nanoscale MD simulations and to macroscale using the frictional heating model. Nanoscale is reported for contact temperature, and macroscale is reported for background temperature.

the friction stress at the nanoscale rests on the atomistic model, which is DC-r^{2}SCAN MLIP in our case. In Supplemental Material [12], we quantify the validity of the DC-r^{2}SCAN MLIP model, showing excellent agreement with density functional theory (DFT) reference and representation of physical properties of water, ice, and amorphous silica. However, a single model may be biased, and the modeling of water using DFT is notoriously difficult [51]. Therefore, we repeated the sweep with force-field simulations using TIP4P/Ice for water and ClayFF for the silica (see Supplemental Material [12] for details). As demonstrated by the parity plot in Fig. 3(a), the force-field-based simulations are in very close agreement with the MLIP, with an R^2 of 0.96, indicating that nanoscale friction behavior is not highly model sensitive. We also computed the friction stress for different orientations of ice planes, first prismatic and second prismatic (FP and SP), which are known to have different premelting behaviors [52,53]. For these, we get an R^2 of 0.99, which is within the statistical noise of sampling. Finally, for contact pressure, there are differences, especially at high temperatures and high contact pressures beyond the penetration hardness (for which structures can fully melt), but for the most part friction stress of the MLIP is largely insensitive to contact pressure, with an R^2 of 0.93, which is in line with contact pressure not playing a major role, except when beyond the penetration hardness. We note that film thickness is more sensitive to model, orientation, and contact pressure than friction stress, as shown in Fig. S7 of Supplemental Material [12]: the force-field films are thicker than the MLIP ones by a median factor of 1.6, and the ratio increases with sliding velocity, even though the friction stresses agree closely. The $R^2_{\log}$ of our estimated coefficient of friction against experiments upscaled from nanoscale friction stress, rests on several assumptions, of which we report the most sensitive ones in Figs. 3(d)–3(f). It is most sensitive to the radius of the ice pebbles, but within the range of experimentally determined values [54], we have 0.8 agreement with experiment. σ_c and σ_P affect $R^2_{\log}$ in a similar manner, scaling the predicted coefficient of friction for low velocities [see Eq. (2)] and all velocities, respectively. Other parameters have smaller effects, as shown in Fig. S8 [12].

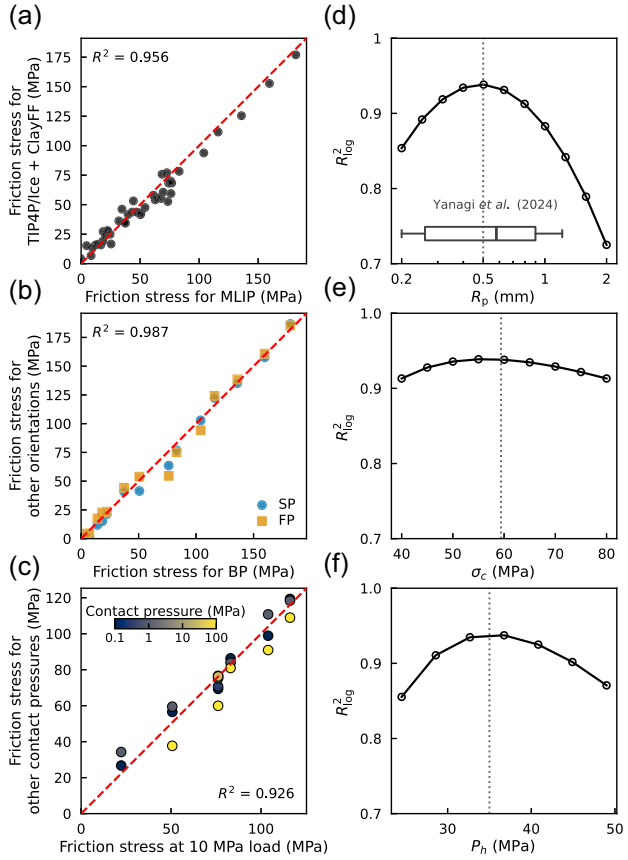


FIG. 3. Robustness of the nano-to-macro friction pipeline. (a) Parity of friction stress between the DC-r^{2}SCAN MLIP and the classical TIP4P/Ice + ClayFF force field at matched basal-plane configurations, paired by velocity and supercooling ΔT from the respective model melting point. (b) Parity of friction stress at the basal plane against the secondary prismatic (SP) and first prismatic (FP) at 10 MPa contact pressure, matched by temperature and sliding velocity. (c) Parity of friction stress at 10 MPa contact pressure against friction stress at other contact pressures spanning 0.1 MPa to 100 MPa, basal plane only. (d)–(f) Log-space coefficient of determination $R^2_{\log}$ of the macroscale friction prediction against the pooled experimental dataset, as the contact radius R_p (d), the friction-stress floor σ_c (e), and the penetration hardness σ_P (f) are varied; vertical dotted lines mark the values adopted in the main analysis. The horizontal box-whisker plot in (d) shows the experimental ice pebble radius range reported by Yanagi *et al.* [54].

Our findings provide a window into reconciling conflicting views on ice friction present in the literature. Baran *et al.* [9,10] highlight shear thinning as important for ice friction. We also observe it in our nanoscale simulations [Fig. 2(b)]. In zero-velocity simulations, premelting alone establishes the initial film between the ice and glass surfaces, and this film holds near 5.5 Å down to −89 °C and thickens from 10 Å to 11 Å within 1 °C of melting in both models [Figs. S7(e)–S7(f) [12]]. Atila *et al.* [11] have shown that at ice-ice interfaces, the film is instead established by displacement-driven amorphization. Which route dominates is set by the counterface: at the hydrophilic ice-glass interface studied here, premelting alone maintains a film at rest, whereas at their ice-ice interface the film recrystallizes when sliding stops, leaving only a few interfacial monolayers, so there the sliding itself must generate the film. Displacement-driven amorphization likely plays a role in thickening our film, which grows by a factor of 2.4 to 3.8 with sliding velocity at a fixed contact temperature [Fig. 2(a)]. That the two routes lead to a similar state is supported structurally: Atila *et al.* characterize their shear-amorphized ice as very close to supercooled water, reporting only minor deviations in the pair

distribution function (see the Supplemental Material of Ref. [11]), and our steady-state O-O $g(r)$ inside the premelting film matches this picture in both models and at every (T, v) probed (Fig. S6 [12]). The two pictures therefore complement each other, with frictional heating governing the friction once the film is established. Atila *et al.* anticipate this, noting that recrystallization slows rapidly as the melting point is approached, so that the film thickens and the frictional heating argument may still hold, "though not to the extent that liquefaction should be attributed to thermal melting." Our model describes frictional heating without thermal melting: it contains no melting enthalpy, and the friction stress in Eq. (1) decreases continuously as $(1 - T/T_m)^\beta$ without a phase transition. The film properties also depend on crystal orientation [52,53] [Fig. 3(b)]. However, even with these effects present, we have shown that nanoscale simulations do not capture the velocity dependence of ice friction [Fig. 1(c)] and that frictional heating is a necessary ingredient to describe the observed velocity dependence qualitatively and quantitatively. Finally, pressure melting is already considered unlikely in most situations as ice asperity contact regions yield by plastic flow before the pressure becomes high enough to form liquid water, and our results corroborate that this is an unnecessary hypothesis to explain the slipperiness of ice: the friction stress only weakly depends on contact pressure under the pressures probed [0.1 MPa to 100 MPa, Fig. 3(c)].

Several aspects of ice friction remain to be explored. The predictions reported here apply to a specific ice-glass counterface and not to ice-on-ice or ice-on-other-material configurations more generally; materials with higher thermal conductivity, such as metals, would lead to different thermal feedback. We have not considered in depth the effects of surface chemistry, such as hydroxylated or hydrophobic surfaces (e.g., waxes used in skiing), snow, ploughing [8], or the formation of ice-particle slurries. Canale *et al.* [6] report a thicker (order ∼100 nm), more viscous interfacial film whose viscosity rise toward the melting point reflects this thick-film regime rather than the velocity dependence of friction that we address. We note, however, that the thickness of even ordinary premelting layers remains contested across experimental techniques, with simulations agreeing more closely [55]. Nevertheless, the velocity dependence of the friction coefficient data by Canale *et al.* (measured for ice against a borosilicate-glass bead, an ice-glass contact) is consistent with our predictions [Fig. 1(f)]. Our macroscale predictions are anchored to experiment at one point: the low-velocity friction floor σ_c, taken from Miyashita *et al.* [42] at $v < 5 \times 10^{-3}$ m s^{-1}. Agreement at these low velocities is therefore expected, whereas agreement at $v \geq 5 \times 10^{-3}$ m s^{-1}, on held-out data from four other experimental sources, is a prediction. The Persson heat model treats the slider as making contact at asperities of a single radius (here $R_p = 0.5$ mm, within the experimental range reported in Ref. [54]); a real ice slider carries a distribution of asperity sizes, with the associated surface roughness and rms slope, that we do not convolve over. The melting point of our DC-r^{2}SCAN MLIP is $T_m = 289$ K, about 16 K above the experimental value, so absolute contact temperatures here should be read relative to T_m. These are promising directions for future work, requiring additional simulations and different theoretical frameworks.

Our analysis focuses on the velocity dependence of ice friction, but as emphasized by Rosenberg, ice is slippery even while standing still [56], potentially at odds with frictional heating hypotheses. For the contacts studied here, this paradox is resolved by the picture that we provide. A premelting film is already present at rest, so the interface is lubricated before anything moves. Frictional heating then makes the ice far more slippery at very modest velocities: movements sustained over the scale of one millimeter, with tangential velocities of ∼0.1 m s^{-1}, warm the contact and lead to dramatic drops in friction. This is qualitatively consistent with everyday experience: slow, careful steps below 0.1 m s^{-1} retain grip, but rapid scuffing to regain grip ends in catastrophe.

Acknowledgments—This work was supported by the Research Council of Norway through the Centre of Excellence Hylleraas Centre for Quantum Molecular Sciences under Grant No. 262695 and the Young Researcher Talent Grants No. 344993 and No. 354100. We acknowledge the EuroHPC Joint Undertaking for awarding this project access to the EuroHPC supercomputer LUMI, hosted by CSC (Finland) and the LUMI consortium through a EuroHPC Regular Access call under Grants No. EHPC-REG-2023R02-088 and No. EHPC-REG-2023R03-146. Support was also received from the Centre for Advanced Study in Oslo, Norway, which funded and hosted the SLB Young CAS Fellow research project during the academic years of 2023–2024 and 2024–2025. Part of the simulations were performed on resources provided by Sigma2—the Norwegian National Infrastructure for High-Performance Computing and Data Storage in Norway, under Grants No. NN4654K and No. NS4654K. Generative AI (Claude Opus, Anthropic) was used to assist with manuscript editing and revision.

The authors declare no competing interests.

Data availability—The data that support the findings of this article are openly available at [57].

[1] R. M. Gramly, *Guide to Palaeolithic Artifacts and Features of the Americas* (Rowman & Littlefield, Lanham, MD, 2024), p. 95.
[2] M. Faraday, Philos. Mag. **17**, 162 (1859).
[3] H. H. G. Jellinek, J. Colloid Interface Sci. **25**, 192 (1967).

[4] J. Joly, Sci. Proc. R. Dublin Soc. **5**, 453 (1887).
[5] F. P. Bowden and T. Hughes, Proc. R. Soc. A **172**, 280 (1939).
[6] L. Canale, J. Comtet, A. Niguès, C. Cohen, C. Clanet, A. Siria, and L. Bocquet, Phys. Rev. X **9**, 041025 (2019).
[7] B. Weber, Y. Nagata, S. Ketzetzi, F. Tang, W. J. Smit, H. J. Bakker, E. H. G. Backus, M. Bonn, and D. Bonn, J. Phys. Chem. Lett. **9**, 2838 (2018).
[8] R. W. Liefferink, F. C. Hsia, B. Weber, and D. Bonn, Phys. Rev. X **11**, 011025 (2021).
[9] Ł. Baran, P. Llombart, W. Rżysko, and L. G. MacDowell, Proc. Natl. Acad. Sci. U.S.A. **119**, e2209545119 (2022).
[10] Ł. Baran and L. G. MacDowell, J. Chem. Phys. **160**, 056101 (2024).
[11] A. Atila, S. V. Sukhomlinov, and M. H. Müser, Phys. Rev. Lett. **135**, 066204 (2025).
[12] See Supplemental Material at http://link.aps.org/supplemental/10.1103/9wv5-ypdm for the simulation models and protocols, the validation of the machine-learning interatomic potential, the analysis protocols, and supplementary analyses of the premelting film and the sensitivity of the upscaled friction coefficient, which includes Refs. [13–40].
[13] S. Dasgupta, E. Lambros, J. P. Perdew, and F. Paesani, Nat. Commun. **12**, 6359 (2021).
[14] S. Dasgupta, G. Cassone, and F. Paesani, J. Phys. Chem. Lett. **16**, 2996 (2025).
[15] S. Dasgupta, S. Saha, and F. Paesani, J. Phys. Chem. Lett. **16**, 11996 (2025).
[16] J. Zeng *et al.*, J. Chem. Phys. **159**, 054801 (2023).
[17] J. Zeng, D. Zhang, A. Peng, X. Zhang, S. He, Y. Wang, X. Liu, H. Bi, Y. Li, C. Cai *et al.*, J. Chem. Theory Comput. **21**, 4375 (2025).
[18] Y. Zhai, A. Caruso, S. L. Bore, Z. Luo, and F. Paesani, J. Chem. Phys. **158**, 084111 (2023).
[19] S. L. Bore and F. Paesani, Nat. Commun. **14**, 3349 (2023).
[20] F. Sciortino, Y. Zhai, S. L. Bore, and F. Paesani, Nat. Phys. **21**, 480 (2025).
[21] Hylleraas Software Platform Developers, "HyAL: Hylleraas Active Learning", https://gitlab.com/hylleraasplatform/hyal (2025).
[22] H. M. Cezar, T. Bodenstein, H. A. Sveinsson, M. Ledum, S. Reine, and S. L. Bore, npj Comput. Mater. **11**, 200 (2025).
[23] M. Matsumoto, T. Yagasaki, and H. Tanaka, J. Comput. Chem. **39**, 61 (2018).
[24] L. C. Erhard, J. Rohrer, K. Albe, and V. L. Deringer, npj Comput. Mater. **8**, 90 (2022).
[25] D. Heyes, E. Smith, D. Dini, and T. Zaki, J. Chem. Phys. **135**, 024512 (2011).
[26] A. Brünger, C. L. Brooks III, and M. Karplus, Chem. Phys. Lett. **105**, 495 (1984).
[27] R. T. Cygan, J.-J. Liang, and A. G. Kalinichev, J. Phys. Chem. B **108**, 1255 (2004).
[28] J. L. F. Abascal, E. Sanz, R. García Fernández, and C. Vega, J. Chem. Phys. **122**, 234511 (2005).
[29] A. P. Thompson, H. M. Aktulga, R. Berger, D. S. Bolintineanu, W. M. Brown, P. S. Crozier, P. J. in 't Veld, A. Kohlmeyer, S. G. Moore, T. D. Nguyen, R. Shan, M. J. Stevens, J. Tranchida, C. Trott, and S. J. Plimpton, Comput. Phys. Commun. **271**, 108171 (2022).
[30] J.-P. Ryckaert, G. Ciccotti, and H. J. C. Berendsen, J. Comput. Phys. **23**, 327 (1977).
[31] A. P. Thompson, S. J. Plimpton, and W. Mattson, J. Chem. Phys. **131**, 154107 (2009).
[32] M. M. Conde, M. Rovere, and P. Gallo, J. Chem. Phys. **147**, 244506 (2017).
[33] M. Holz, S. R. Heil, and A. Sacco, Phys. Chem. Chem. Phys. **2**, 4740 (2000).
[34] A. J. Easteal, W. E. Price, and L. A. Woolf, J. Chem. Soc. Faraday Trans. **85**, 1091 (1989).
[35] R. Mills, J. Phys. Chem. **77**, 685 (1973).
[36] E. W. Lemmon, M. O. McLinden, and D. G. Friend, in *NIST Chemistry WebBook*, edited by P. Linstrom and W. Mallard (National Institute of Standards and Technology, Gaithersburg, MD, 2021).
[37] A. Dehaoui, B. Issenmann, and F. Caupin, Proc. Natl. Acad. Sci. U.S.A. **112**, 12020 (2015).
[38] A. Musaelian, S. Batzner, A. Johansson, L. Sun, C. J. Owen, M. Kornbluth, and B. Kozinsky, Nat. Commun. **14**, 579 (2023).
[39] P. M. Larsen, S. Schmidt, and J. Schiøtz, Model. Simul. Mater. Sci. Eng. **24**, 055007 (2016).
[40] A. Stukowski, Model. Simul. Mater. Sci. Eng. **18**, 015012 (2009).
[41] B. N. J. Persson, J. Chem. Phys. **143**, 224701 (2015).
[42] N. Miyashita, A. E. Yakini, W. Pyckhout-Hintzen, and B. N. J. Persson, J. Chem. Phys. **158**, 174702 (2023).
[43] M. Akkok, C. M. McC. Ettles, and S. J. Calabrese, J. Tribol. **109**, 552 (1987).
[44] A. R. Penner, Am. J. Phys. **69**, 332 (2001).
[45] H. Nyberg, S. Alfredson, S. Hogmark, and S. Jacobson, Wear **301**, 583 (2013).
[46] J. A. Greenwood, Wear **150**, 153 (1991).
[47] M. M. Miranda, C. R. Matos, N. V. Rodrigues, A. J. S. C. Pereira, and J. J. Costa, J. Iber. Geol. **45**, 147 (2019).
[48] P. V. Hobbs, *Ice Physics* (Clarendon Press, Oxford, 1974).
[49] L. Pastewka, S. Moser, P. Gumbsch, and M. Moseler, Nat. Mater. **10**, 34 (2011).
[50] G. Moras, A. Klemenz, T. Reichenbach, A. Gola, H. Uetsuka, M. Moseler, and L. Pastewka, Phys. Rev. Mater. **2**, 083601 (2018).
[51] M. J. Gillan, D. Alfè, and A. Michaelides, J. Chem. Phys. **144**, 130901 (2016).
[52] M. M. Conde, C. Vega, and A. Patrykiejew, J. Chem. Phys. **129**, 014702 (2008).
[53] J. R. Espinosa, C. Vega, and E. Sanz, J. Phys. Chem. C **120**, 8068 (2016).
[54] S. Yanagi, T. Kameda, Y. Harada, and K. Sado, Sci. Rep. **14**, 11463 (2024).
[55] B. Slater and A. Michaelides, Nat. Rev. Chem. **3**, 172 (2019).
[56] R. Rosenberg, Phys. Today **58**, No. 12, 50 (2005).
[57] S. L. Bore, B. N. J. Persson, and H. A. Sveinsson, Why ice is so slippery, Zenodo (2026), 10.5281/zenodo.20407641.
[58] B. N. J. Persson, A. I. Volokitin, and H. Ueba, J. Phys. Condens. Matter **23**, 045009 (2011).
[59] J. Li, S. Li, W. Zhang, B. Wei, and Q. Yang, Lubricants **10**, 265 (2022).
[60] D. T. Limmer and D. Chandler, J. Chem. Phys. **141**, 18C505 (2014).

End Matter

Frictional heating modeling—We determine the contact temperature at the ice surface and the slider due to frictional heating as follows. We assume that the slider is flat and that it makes contact with the ice substrate only at isolated pebble-shaped asperities of radius R_p. These asperities make up only a small proportion of the apparent contact area, as illustrated in Fig. 1(d). Because of frictional heating, there will be an increase ΔT of the contact temperature T with respect to the background temperature T_0. Seen from the slider, the contacts with the ice pebbles of the substrate are disk-shaped moving heat sources that provide a heat flux J. The maximum temperature increase within the contact region is, in this case, very well approximated by Eq. (8) in Ref. [46]:

$$\Delta T = \frac{s(v) J R_p}{\kappa_{\text{slider}}} \left(1 + \frac{\pi}{8} \frac{R_p v}{D_{\text{slider}}}\right)^{-1/2}, \tag{A1}$$

where D is the thermal diffusivity, κ is the thermal conductivity, and s is the proportion of the heat that goes into the slider (the rest, $1 - s$, goes into the ice). This expression includes both the effect of normal heat transfer away from the contact and the effect of new cold glass constantly entering the contact region. It is useful to write Eq. (A1) as

$$s(v) J = \alpha_{\text{slider}} \Delta T$$

with

$$\alpha_{\text{slider}} = \frac{\kappa_{\text{slider}}}{R_p} \left(1 + \frac{\pi}{8} \frac{R_p v}{D_{\text{slider}}}\right)^{1/2}.$$

For the substrate, with stationary ice pebbles, the maximum temperature elevation is [46]

$$\Delta T = \frac{[1 - s(v)] J R_p}{\kappa_{\text{substrate}}},$$

or equivalently

$$[1 - s(v)] J = \alpha_{\text{substrate}} \Delta T,$$

with

$$\alpha_{\text{substrate}} = \frac{\kappa_{\text{substrate}}}{R_p}.$$

We approximate the temperatures on the ice surface and the silica glass surface to be equal (i.e., the contact temperature) [58]. We thus obtain the partitioning coefficient of the heat flux:

$$s(v) = \frac{\alpha_{\text{slider}}}{\alpha_{\text{substrate}} + \alpha_{\text{slider}}}. \tag{A2}$$

This partitioning tends toward 0.5 for stationary contacts between materials with similar thermal properties, whereas it tends toward 1 at high sliding velocities, meaning that almost all the heat goes into the slider. Using the MD-derived friction law in Eq. (1), we insert $J = \sigma_f v$ into Eq. (A1) to recover the contact temperature relation given in Eq. (4). Since σ_f is a function of the contact temperature, Eq. (4) is an implicit equation for the contact temperature T in the region. We solve it iteratively and then obtain σ_f from the same constitutive relations. Note that we do not consider squeeze-out of the premelting film as, for nanometer-thick films at macroscopic contact dimensions, squeeze-out is negligible even at the low viscosity of water. In addition, during sliding, shear-induced amorphization would continuously produce a liquidlike film on the ice surface [11].

To obtain friction stresses for comparison with experiments, we insert parameters taken from the curling literature, because typical curling ice has been very well characterized; it is pebbled with a contact diameter of around 2 mm [59]. To obtain roughly the midpoint temperature instead of the maximum temperature of the contacts, we set $R_p = 0.5$ mm. Curling stones have a very flat contact surface, which is consistent with the heat model described above. These stones are made of granite, which is mostly a silicate mineral, for which our amorphous silica glass is a reasonable analog. In the frictional heating model, we use thermal properties of the ice and granite as listed in Table I. We compute the thermal diffusivity needed in Eq. (4) by $D = \kappa/(\rho C_P)$.

Friction coefficient—Relating the frictional shear stress to the friction coefficient is nontrivial because it depends on whether the surfaces deform elastically (as expected for sufficiently smooth surfaces) or plastically. Plastic deformation of ice is a stress-aided, thermally activated process, and the penetration hardness of ice depends on the temperature and the indentation velocity. Here we note that, if a slider is slid repeatedly on ice, the high ice asperities will be smoothed plastically during the first few sliding events, so after run-in, the surfaces may deform only elastically and are subject to a contact pressure on the order of the penetration hardness of ice of about $\sigma_P = 35$ MPa, collected from experimental data [44,48]. We then compute the friction coefficient $\mu = \sigma_f/\sigma_P$.

Ice-glass friction model parameterization—We represent our nanoscale MD data by analytical functions parameterized based on nanoscale ice-glass friction data

at specific state points. The melting points of our water models differ from the experimental one: 289 K for DC-r^{2}SCAN and 270 K for TIP4P/Ice + ClayFF. We therefore report temperatures in °C relative to the melting point of the model concerned, to enable comparison with experimental data. For Eq. (1), the four parameters are determined by an iterative cofit with a strict train-validate split. σ_k, v_k, and β are anchored to nanoscale MD friction-stress data at 10 MPa contact pressure; the low-velocity floor σ_c is anchored to ice-glass friction-coefficient data of Miyashita *et al.* [42] restricted to $v < 5 \times 10^{-3}$ m s^{-1} ($n = 28$ points), where Eq. (1) reduces to Eq. (2) within ~5%. The iteration alternates (i) refitting (σ_k, v_k, β) on the MD data with σ_c pinned and (ii) refitting σ_c on the 28 Miyashita low-velocity points with (σ_k, v_k, β) pinned; it converges in two iterations to the values quoted above ($\sigma_c = 59$ MPa, $\sigma_k = 391$ MPa, $v_k = 0.53$ m s^{-1}, $\beta = 0.61$). The held-out validation pool used for the $R^2_{\log} = 0.88$ reported in the main text consists of all macroscale experimental points from Akkok, Penner, Nyberg, and Canale at $v \geq 5 \times 10^{-3}$ m s^{-1} ($n = 55$); the training set and validation pool have zero source overlap and zero velocity-range overlap. Parity plots of how well the model predictions match the MD data are shown in Fig. 4(a), and plots of how macroscale predictions match the experimental friction coefficient are in Fig. 4(b). For the premelting film thickness, we fitted the following functional form for simulations with temperatures between 260 and 289 K:

$$h(v,T) = h_0 + a\left[-\ln\left(1 - \frac{T}{T_m}\right)\right]^{\gamma}\left(1 + \frac{v}{v_0}\right). \quad \text{(C1)}$$

The offset is held fixed at $h_0 = 0.60$ nm. The remaining parameters, $a = 13.06$ pm, $\gamma = 2.37$, and $v_0 = 5.06$ m s^{-1}, are fitted to MD data for premelting film thickness as a function of temperature and sliding velocity, with the parity plot in Fig. 4(c). We note that Limmer and Chandler proposed such a logarithmic dependence for temperature for premelting thickness in ice-air [60], albeit without γ exponent. A parity plot of how well the model predictions match the MD data is reported in Fig. 4(c). Equation (C1) is plotted in Fig. 2(a), with premelting film viscosity in Fig. 2(b) computed using $\eta = \sigma_f h/v$.

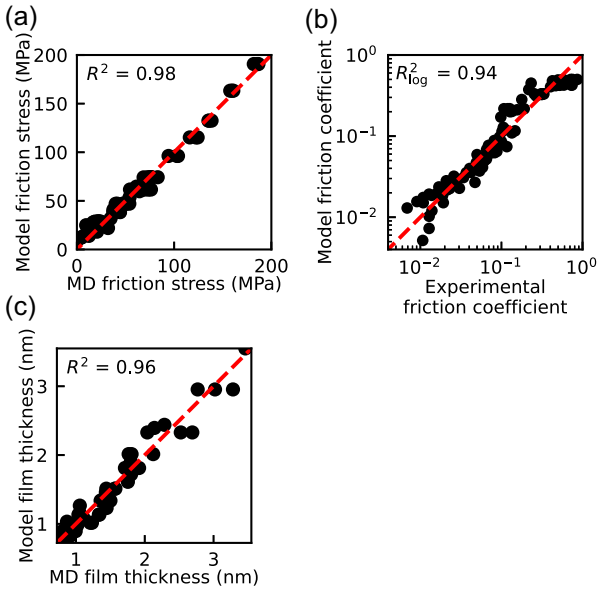


FIG. 4. Parity plots for ice-glass friction modeling vs data. (a) Nanoscale MD data vs fitted model predictions for friction stress Eq. (1), corresponding to Fig. 1(b). (b) Experimental vs modeled macroscale friction coefficient, corresponding to Fig. 1(f): all $n = 88$ experimental points ($R^2_{\log} = 0.94$; $R^2_{\log} = 0.88$ on the $n = 55$ held-out validation points). (c) MD data vs fitted model predictions for premelting film thickness, corresponding to Fig. 2(a).